

Learning to Dial-a-Ride: A Deep Graph Reinforcement Learning Approach to the Electric Dial-a-Ride Problem

Sten Elling Tingstad Jacobsen^{a,b,*,1}, Attila Lischka^a, Balázs Kulcsár^a and Anders Lindman^b

^aDepartment of Electrical Engineering, Chalmers University of Technology, Gothenburg, Sweden

^bVolvo Cars, Gothenburg, Sweden

ARTICLE INFO

Keywords:

Electric Dial-a-Ride problem
Energy-Aware Vehicle Routing
Deep Reinforcement Learning
Graph Neural Networks
Mobility-on-Demand

ABSTRACT

Urban mobility systems are transitioning toward electric, on-demand services, creating operational challenges for fleet management under energy and service-quality constraints. The Electric Dial-a-Ride Problem (E-DARP) extends the classical dial-a-ride problem by incorporating limited battery capacity and nonlinear charging dynamics, increasing computational complexity and limiting the scalability of exact methods for real-time use. This paper proposes a deep reinforcement learning approach based on a graph neural network encoder and an attention-driven route construction policy. By operating directly on edge attributes such as travel time and energy consumption, the method captures non-Euclidean, asymmetric, and energy-dependent routing costs in real road networks. The learned policy jointly optimizes routing, charging, and service quality without relying on Euclidean assumptions or handcrafted heuristics. The approach is evaluated on two case studies using ride-sharing data from San Francisco. On benchmark instances, the method achieves solutions within 0.4% of best-known results while reducing computation times by orders of magnitude. A second case study considers large-scale instances with up to 250 request pairs, realistic energy models, and nonlinear charging. On these instances, the learned policy outperforms Adaptive Large Neighborhood Search (ALNS) by 9.5% in solution quality while achieving 100% service completion, with sub-second inference times compared to hours for the metaheuristic. Finally, sensitivity analyses quantify the impact of battery capacity, fleet size, ride-sharing capacity, and reward weights, while robustness experiments show that deterministically trained policies generalize effectively under stochastic conditions.

1. Introduction

Urban transportation systems are undergoing major changes as cities adopt electric vehicles, autonomous driving, and on-demand services. More than half of the world's population now lives in cities, and this share is expected to reach 68% by 2050 [1]. This rapid urbanization creates growing pressure on transportation networks to reduce emissions, ease congestion, and provide accessible mobility for all residents [2]. Transportation currently produces nearly a quarter of global energy-related CO₂ emissions [3], making cleaner mobility solutions essential for climate action. Fleets of electric autonomous vehicles offer a way to address these challenges by combining zero-emission transportation with intelligent coordination for efficient, on-demand services [4, 5]. However, operating such systems requires solving complex optimization problems that coordinate vehicle routes, passenger assignments, and battery charging in real time, challenges that intensify as fleets grow larger and serve wider areas [6, 7].

The Electric Dial-a-Ride Problem (E-DARP) extends the classical Dial-a-Ride Problem by incorporating electric vehicle constraints such as limited driving range and charging requirements. Originally introduced as a generalization for electric and autonomous fleets [8], the E-DARP is characterized by its focus on passenger transportation with user-centric service quality constraints: time windows that bound when service can begin, maximum ride time limits that constrain how long passengers spend in vehicles, and precedence requirements ensuring pickups occur before deliveries. These constraints, combined with vehicle capacity limits and battery feasibility requirements, create a computationally challenging problem. Even without electric constraints, the classical DARP is NP-hard, and a single vehicle serving n requests admits $(2n)!/2^n$ distinct precedence-feasible orderings—approximately 2.38×10^{18}

*Corresponding author

**Principal corresponding author

✉ elling@chalmers.se (S.E.T. Jacobsen); lischka@chalmers.se (A. Lischka); kulcsar@chalmers.se (B. Kulcsár); anders.lindman@volvocars.com (A. Lindman)

ORCID(s):

sequences for just $n = 10$ requests [9]. The integration of nonlinear charging dynamics and energy-dependent routing further compounds this complexity.

Exact optimization methods for dial-a-ride problems have progressed significantly, with branch-and-cut [10, 11] and branch-and-price approaches [12, 13] solving classical DARP instances with up to 8 vehicles and 96 requests. Recent work has extended these methods to electric vehicle settings: [14] developed granular tabu search for the E-PDPTW with partial recharging, [15] proposed robust optimization for demand uncertainty, and most recently, [16] introduced the first branch-and-price algorithm specifically for E-DARP using fragment-based representations and novel labeling techniques. Despite these advances, the combinatorial complexity introduced by time windows, capacity limits, ride-time constraints, and nonlinear charging dynamics renders exact methods computationally prohibitive for large-scale, real-time applications requiring sub-second response times. These scalability challenges have motivated growing interest in learning-based approaches. Deep reinforcement learning (DRL) has emerged as a promising paradigm for combinatorial optimization, offering an unsupervised learning approach that discovers effective policies through trial-and-error interaction rather than requiring labeled solutions from existing solvers [17]. Foundational work on attention mechanisms [18, 19] demonstrated viability for vehicle routing [20, 21]. The POMO framework [22] showed that learned policies can match or exceed classical heuristics by exploiting multiple solution trajectories during training—an approach particularly relevant to E-DARP where sequential decision structure and robust policy learning align well with POMO's design. Extensions to pickup-and-delivery problems have introduced heterogeneous attention mechanisms respecting precedence constraints [23] and symmetric architectures exploiting paired location structure [24]. However, these methods primarily address basic PDP or PDPTW without energy constraints, leaving the integration of battery management and charging decisions largely unexplored in the learning-based literature.

Despite advances in both exact methods and DRL, the application of learning-based approaches to energy-aware dial-a-ride problems remains limited. Supervised learning approaches require large datasets of high-quality solutions generated by existing solvers, creating a computational bottleneck and limiting applicability to problem variants where efficient solvers exist [18]. Most DRL research addresses either conventional DARP or electric vehicle routing without ride-time constraints [25, 26]. Notable exceptions include [27], who apply safe reinforcement learning to dynamic stochastic electric vehicle routing, though without the passenger-centric constraints of dial-a-ride. Meanwhile, optimization-based E-DARP literature [8, 16] provides valuable benchmarks but requires computation times unsuitable for real-time deployment and does not scale.

At the same time, applying DRL to E-DARP presents distinct challenges. First, the combination of passenger time windows, vehicle capacity, ride-time limits, and battery constraints creates a complex constraint structure that standard neural architectures struggle to represent effectively. Second, and crucially, the E-DARP with energy-dependent routing is inherently a non-Euclidean problem: energy consumption depends on factors such as vehicle load, terrain, and traffic conditions that cannot be captured by coordinate-based distance calculations. Standard attention-based architectures for vehicle routing [21, 22] typically embed node locations as Euclidean coordinates and derive edge features (distances, travel times) from these coordinates. This approach fundamentally cannot represent asymmetric travel times, asymmetric real world energy consumption, or real-world road network structures which are asymmetric. Consequently, node-based graph neural networks and standard attention mechanisms are ill-suited for learning effective policies in energy-aware routing problems. Third, while DRL has shown promise on synthetic Euclidean benchmarks, scalability to operationally meaningful instance sizes with realistic, non-Euclidean cost structures remains underexplored. Most existing work evaluates on instances with fewer than 100 requests, leaving a gap between academic benchmarks and the larger problems encountered in practice. Finally, the interpretability and transparency of learned policies presents an ongoing challenge. Neural network-based approaches are often criticized as black-box models, making it difficult to understand why specific routing or charging decisions are made [28, 29]. In safety-critical transportation applications, this opacity can hinder trust, regulatory acceptance, and debugging of failure cases [30]. While attention mechanisms offer some degree of interpretability by revealing which problem elements influence decisions [31, 21], systematic frameworks for explaining DRL policies in vehicle routing remain underdeveloped [32]. Recent work has made progress through post-hoc explanation methods [33], mechanistic interpretability of neural routing solvers [34], and interpretable policy architectures [35], suggesting that learning-based methods are becoming increasingly amenable to interpretation, though this remains an active area of research beyond the scope of the present work.

This work applies the GREAT (Graph Edge Attention Network) encoder architecture [36] to the E-DARP within an unsupervised deep reinforcement learning framework. Unlike supervised approaches that require optimal or near-optimal solutions for training, our method learns routing policies entirely through reward-driven exploration,

eliminating dependence on existing solvers and enabling application to problem scales and variants where generating training labels would be computationally prohibitive. GREAT is specifically designed to address the non-Euclidean nature of real-world routing problems. Whereas conventional node-based architectures derive edge information from node coordinates, GREAT operates directly on edges: information is compared between and passed along edges sharing endpoints, with edge features serving as the primary inputs to the attention mechanism. This edge-centric design is critical for energy-dependent routing, where edge features such as travel times and energy consumption are given directly from road network data rather than being computed from Euclidean coordinates. The architecture can naturally represent asymmetric costs (different energy consumption in each direction), and asymmetric graph structures. For the E-DARP, routing decisions correspond to selecting edges (transitions between pickup locations, delivery locations, and charging stations), making GREAT’s edge-based formulation a natural fit. The representation captures the problem’s intrinsic structure, encoding battery constraints through energy-consumption edge features, time windows through temporal feasibility features, and ride-time restrictions through service-time attributes, without requiring auxiliary constraint-encoding mechanisms or coordinate-based approximations.

The main contributions of this study are threefold:

1. **Unsupervised learning framework with edge-based neural architecture.** We demonstrate that the GREAT encoder architecture, combined with deep reinforcement learning, enables fully unsupervised learning of E-DARP routing policies. The model discovers effective strategies through reward-driven exploration without requiring labeled solutions from optimization algorithms. By processing routing problems through edge-level attention rather than node-based representations and operating directly on edge features (travel times, distances, energy consumption), the architecture naturally handles asymmetric costs and non-Euclidean network structures that characterize real-world electric vehicle routing. This design choice, combined with an attention-based decoder and POMO training, enables the policy to learn sophisticated routing and charging strategies.
2. **Computational efficiency at scale.** On benchmark instances, our method achieves optimal solutions (0.0% gap) for problems with up to 30 requests and maintains near-optimal quality (0.4% gap) for 50-request instances, while providing computational speedups of 20 \times to over 7,000 \times compared to exact methods. Through curriculum learning, the approach scales to instances with 250 request pairs (500 nodes), problem sizes where exact E-DARP solvers become computationally prohibitive, while maintaining sub-second inference times suitable for real-time fleet management. This computational profile enables dynamic re-optimization in response to new requests, traffic conditions, or vehicle availability changes.
3. **Comprehensive sensitivity analysis across operational, algorithmic, and environmental factors.** We conduct systematic analyses examining: (i) operational attributes, including battery capacity (20 to 40 kWh), fleet size (4 to 8 vehicles), and ride-sharing capacity (1 to 3 passengers), revealing that larger batteries achieve 6 to 15% higher profits, 8-vehicle fleets are necessary for guaranteed coverage, and ride-sharing introduces predictable lateness trade-offs; (ii) reward function weights, demonstrating that adequate completion incentives are essential for full service coverage while excessive operational cost penalties lead to conservative behavior and incomplete service; (iii) hyperparameters, identifying that smaller neural architectures (hidden dimension 64 to 128) match or outperform larger models while converging faster; and (iv) robustness under stochastic travel times and energy consumption, showing that deterministic training produces policies generalizing effectively to 10% operational uncertainty.

Together, these contributions demonstrate the potential of learning-based, edge-centric models to tackle large-scale, energy-aware routing problems efficiently and adaptively, providing a practical framework for real-world autonomous fleet deployment. The remainder of this paper is organized as follows. We begin by formulating the E-DARP as a Markov Decision Process and providing a detailed mathematical problem statement including constraints and objectives (Section 2). The methodology is then presented, describing the GREAT encoder architecture, the attention-based decoder, feasibility masking, and the reward function design (Section 3). Next, we detail the experimental setup, including problem instance generation, training procedures, and baseline methods for both benchmark and large-scale case studies (Section 4). Comprehensive results and analysis follow, covering benchmark performance comparison against exact methods, large-scale curriculum learning evaluation, sensitivity analysis across battery sizes, fleet configurations, and ride-sharing capacities, hyperparameter analysis, reward weight sensitivity, and robustness evaluation under stochastic conditions (Section 5). Finally, we conclude with a summary of findings, discussion of limitations, and directions for future research (Section 6).

2. Electric Dial-a-Ride Problem: Definition and Formulation

This section formulates the Electric Dial-a-Ride Problem for deep reinforcement learning. We present a motivating example illustrating the problem’s computational challenges (Section 2.1), formulate the sequential decision-making process as a Markov Decision Process (Section 2.2), and provide a detailed mathematical specification of constraints and objectives (Section 2.3).

2.1. Introductory Example

To illustrate the computational challenges of the Electric Dial-a-Ride Problem (E-DARP), consider a representative instance with seven electric vehicles serving 100 customer requests over a 12-hour planning horizon. Each vehicle has a 40 kWh battery, a maximum capacity of three passengers, and access to ten charging stations distributed across the service area. The objective is to construct feasible vehicle routes that serve all requests while minimizing energy consumption, waiting time, and passenger ride time. Fig. 1 illustrates a solution to such an instance.

Even this seemingly moderate scenario presents fundamental challenges that make the problem computationally difficult. The first challenge is combinatorial explosion: the number of feasible solutions grows exponentially with the number of requests. Even under highly simplified assumptions where each of the 100 requests can be assigned to one of seven vehicles or left unserved, there are at least $8^{100} \approx 1.3 \times 10^{90}$ possible assignment combinations. For any fixed assignment, the number of feasible pickup-delivery sequences grows factorially; even for a single vehicle serving n requests, there are $(2n)!/2^n$ precedence-feasible orderings [9]. Accounting for multiple vehicles, time windows, capacity limits, battery constraints, and charging decisions imposes further restrictions this solution space [8]. The second challenge is the tight coupling between routing and charging decisions [25, 26]. A vehicle may choose to charge early, incurring idle time that delays service, or serve nearby requests first, risking battery depletion and infeasibility later in the route. Greedy strategies that select the nearest feasible request can strand vehicles in low-demand areas with insufficient battery to reach charging stations or complete additional requests [37]. The third challenge is real-time requirements: dynamic fleet operations must repeatedly recompute decisions as new requests arrive and conditions change [38]. Exact mixed-integer optimization methods often require minutes to hours for instances of this size [16, 13], making them unsuitable for real-time deployment.

These challenges motivate our approach of formulating the E-DARP as a Markov Decision Process, where an agent learns to construct vehicle routes through sequential decisions that balance service quality, battery management, and operational efficiency without exhaustive enumeration of the solution space.

2.2. Markov Decision Process Formulation

The E-DARP can be represented as a Markov Decision Process (MDP) denoted by $\mathcal{M} = (\mathcal{S}, \mathcal{A}, \mathcal{R}, \mathcal{T}, H)$. This formulation encompasses the state space \mathcal{S} with states $s_t \in \mathcal{S}$, the action space \mathcal{A} with actions $a_t \in \mathcal{A}$, the reward function $\mathcal{R}(\cdot)$, the transition function $\mathcal{T}(\cdot)$, and the horizon H indicating the episode duration. The state of a problem instance encodes the current vehicle’s operational status (location, time, battery level, passenger load) and the set of served requests, where the next state s_{t+1} is determined by applying the chosen action a_t (selecting the next node to visit) to the current state s_t . An agent is introduced in the MDP to construct solutions by learning a policy $\pi_\theta(a|s)$. The standard objective in reinforcement learning seeks a policy that generates a trajectory ξ maximizing the expected reward: $\pi^* = \arg \max_{\pi_\theta} \mathbb{E}_{\xi \sim \pi_\theta} [\mathcal{R}(\xi)]$. Let $C(\xi)$ denote the total cost and $\mathcal{P}(\xi)$ the total profit associated with trajectory ξ ; the reward is then defined as $\mathcal{R}(\xi) = \mathcal{P}(\xi) - C(\xi)$, assigned at episode termination. However, real-world applications typically allow generating multiple candidate solutions rather than committing to a single trajectory. For combinatorial optimization problems, the learning objective should therefore maximize the best solution among K attempts: $\pi^* = \arg \max_{\pi_\theta} \mathbb{E}_{\xi_i \sim \pi_\theta} [\max_{i=1, \dots, K} \mathcal{R}(\xi_i)]$. This multi-shot formulation motivates learning diverse policies that maintain sufficient exploration across solution attempts, allowing the model to discover high-quality solutions with high probability rather than converging prematurely to a single deterministic trajectory.

2.3. Combinatorial Optimization Formulation

We formulate the E-DARP as a combinatorial optimization problem that determines vehicle routes, service times, and charging decisions to minimize operational costs while satisfying passenger service requirements and electric vehicle constraints. An E-DARP instance with n transportation requests is defined on a directed graph $G = (V, E)$ where $V = \{0\} \cup P \cup D \cup F$ comprises the depot (node 0), pickup nodes $P = \{1, \dots, n\}$, delivery nodes $D = \{n+1, \dots, 2n\}$, and charging stations F . Each request $i \in \{1, \dots, n\}$ pairs pickup node i with delivery node $n+i$. Edges $(i, j) \in E$ are characterized by travel time δ_{ij} , distance d_{ij} , and energy consumption ε_{ij} . Nodes $i \in P \cup D \cup F$

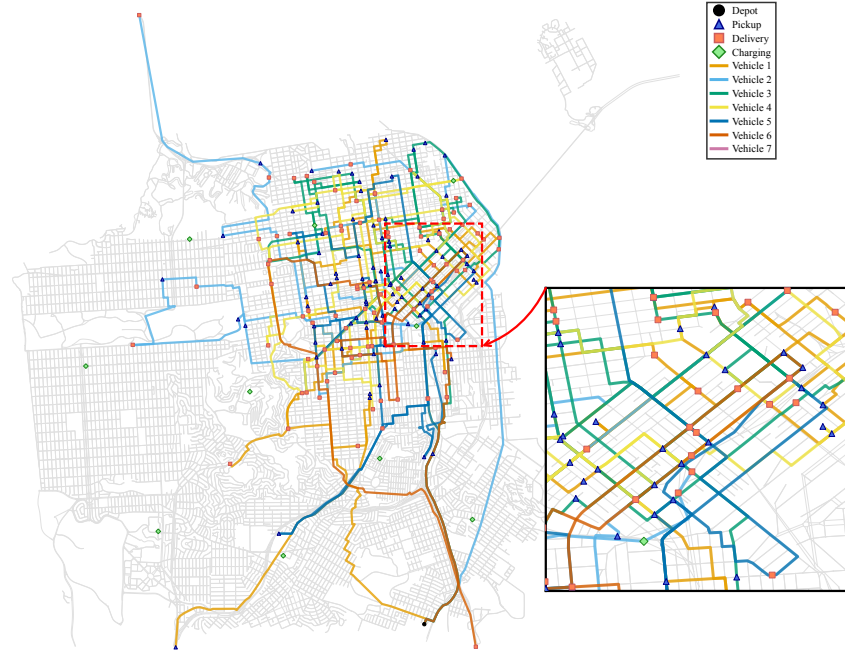


Figure 1: Example E-DARP solution with seven vehicles serving pickup-delivery requests and visiting charging stations in San Francisco.

have service time σ_i and time window $[a_i, \ell_i]$. Pickup nodes have passenger load $q_i > 0$ (removed at corresponding delivery), and requests impose maximum ride time \bar{L}_i . A fleet of K homogeneous electric vehicles operates from the depot, each with passenger capacity Q and battery capacity B . Let $\rho^k = (v_0^k, v_1^k, \dots, v_{T_k}^k)$ denote the route for vehicle k , where $v_t^k \in V$ is the node visited at position t with $v_0^k = v_{T_k}^k = 0$. Let $t_t^k \in \mathbb{R}_+$ denote the service start time and $b_t^k \in [0, 1]$ the state of charge after visiting node v_t^k . The variable l_t^k denotes the current onboard passenger load of vehicle k at step t , while q_i represents the load change incurred when visiting node i (positive for pickups and negative for deliveries). The objective function combines energy consumption, passenger waiting time at pickups, and delivery lateness:

$$J_e(\{\rho^k\}) = \sum_{k=1}^K \sum_{t=0}^{T_k-1} \varepsilon_{v_t^k v_{t+1}^k}, \quad (1)$$

$$J_w(\{\rho^k\}) = \sum_{k=1}^K \sum_{t: v_t^k \in P} \max(0, a_{v_t^k} - t_{t-1}^k - \delta_{v_{t-1}^k v_t^k}), \quad (2)$$

$$J_l(\{\rho^k\}) = \sum_{k=1}^K \sum_{t: v_t^k \in D} \max(0, t_t^k - \ell_{v_t^k}), \quad (3)$$

yielding the total cost $J(\{\rho^k\}) = w_e J_e + w_w J_w + w_l J_l$, where $w_e, w_w, w_l \geq 0$ are weight parameters. The optimization problem is:

$$\underset{\{\rho^k\}_{k=1}^K, \{t_t^k\}, \{b_t^k\}}{\text{minimize}} \quad J(\{\rho^k\}) \quad (4a)$$

$$\text{s.t.} \quad n_{\text{served}}(\{\rho^k\}) = n, \quad (4b)$$

$$i, n+i \in \bigcup_{k=1}^K \rho^k, \quad i < n+i \quad \forall i \in \{1, \dots, n\}, \quad (4c)$$

$$0 \leq \sum_{s=1}^t q_{v_s^k} \leq Q \quad \forall k, \forall t, \quad (4d)$$

$$t_{t+1}^k = \max(t_t^k + \delta_{v_t^k v_{t+1}^k}, a_{v_{t+1}^k}) + \sigma_{v_{t+1}^k} \quad \forall k, \forall t, \quad (4e)$$

$$a_{v_t^k} \leq t_t^k \leq \ell_{v_t^k} \quad \forall k, \forall t, \quad (4f)$$

$$t_{t'}^k - t_t^k \leq \bar{L}_i \quad \forall i, k : v_t^k = i, v_{t'}^k = n+i, \quad (4g)$$

$$b_{t+1}^k = b_t^k - \varepsilon_{v_t^k v_{t+1}^k} / B + \Delta_{t+1}^k \quad \forall k, \forall t, \quad (4h)$$

$$0 \leq b_t^k \leq 1 \quad \forall k, \forall t, \quad (4i)$$

$$b_0^k = 1 \quad \forall k, \quad (4j)$$

$$\Delta_t^k = \begin{cases} P^c(b_{t-1}^k) \sigma_{v_t^k} / B, & v_t^k \in F, \\ 0, & \text{otherwise,} \end{cases} \quad \forall k, \forall t. \quad (4k)$$

where the charging power function is:

$$P^c(b_t) = \begin{cases} 100 \text{ kW} & \text{if } b_t < 0.45 \\ 100 - 140 \cdot (b_t - 0.45) \text{ kW} & \text{if } 0.45 \leq b_t \leq 0.95 \\ 30 \text{ kW} & \text{if } b_t > 0.95 \end{cases} \quad (5)$$

Constraint (4b) enforces complete service coverage by requiring that all n requests are served. Constraint (4c) ensures that each request is served with its pickup preceding the corresponding delivery. Vehicle capacity limits are imposed by Constraint (4d), which bounds the onboard passenger load at all times. Temporal feasibility is enforced through Constraints (4e) and (4f), which define service time propagation along routes and ensure adherence to node time windows. Passenger service quality is controlled by Constraint (4g), which limits the maximum ride time for each request. Battery dynamics are governed by Constraints (4h)–(4k), modeling energy consumption during travel, charging at stations, initial battery conditions, and state-of-charge bounds. For the reinforcement learning formulation, we relax the hard service requirement to accommodate resource-constrained scenarios where battery capacity or fleet size may be insufficient to serve all requests. The reward function becomes:

$$\mathcal{R}(\{\rho^k\}) = -J(\{\rho^k\}) + w_c \cdot n_{\text{served}}(\{\rho^k\}) \quad (6)$$

where $J(\{\rho^k\})$ is the objective value in Eq. (4) and $w_c \geq 0$ weights the completion bonus. This formulation converts the hard constraint $n_{\text{served}}(\{\rho^k\}) = n$ into a soft objective that incentivizes maximum service coverage while allowing partial solutions when constraints prevent serving all demand. The agent receives $\mathcal{R}(\{\rho^k\})$ only at episode termination. Fig. 2 illustrates an example solution, and Table 1 summarizes notation.

3. Methodology

We solve the E-DARP using deep reinforcement learning with a neural network policy that constructs routes iteratively. The neural network encoder processes the problem instance structure (Section 3.1), while an attention-based decoder selects nodes to visit (Section 3.2). We enforce feasibility through action masking rules (Section 3.3) and define the training objective based on solution cost (Section 3.4).

3.1. Problem Encoder

We use the GREAT (Graph Edge Attention Network) encoder [36] to process the problem instance into node embeddings. GREAT is a graph neural network that performs edge-level message passing rather than traditional node-level operations. This design is particularly well-suited for routing problems since such problems are typically defined

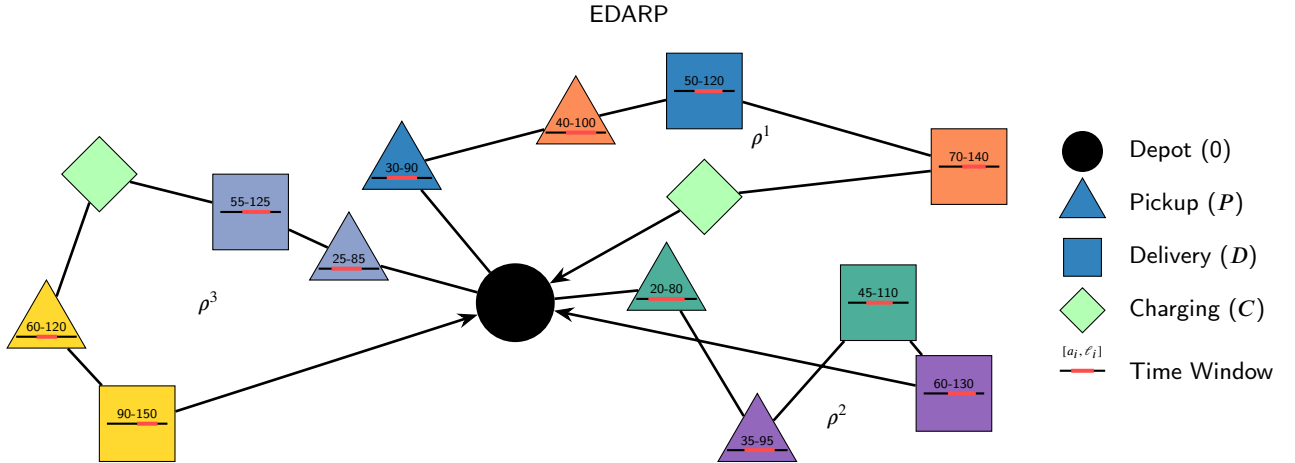


Figure 2: Example E-DARP solution with three vehicle routes and time windows. The depot (node 0) is shown as a filled black circle. Each request i consists of a pickup node $i \in P$ (triangle) and delivery node $n + i \in D$ (square) in matching colors. Black horizontal bars represent the planning horizon for each node, while the overlaid red bars indicate the feasible service time windows $[a_i, e_i]$ during which the vehicle must arrive. Green diamonds represent charging stations $f \in F$ that are available throughout the planning horizon. Routes ρ^1 and ρ^3 include charging stops to maintain battery feasibility throughout their journeys. Each vehicle can carry up to Q passengers simultaneously while respecting both time window constraints and passenger ride time limits.

by graph edge attributes. For example, such characterizing edge features are distance, travel time or expected energy consumption when traveling between a pair of nodes.

In particular, for a given E-DARP instance, we build an edge-based graph the following way: For each node $i \in V$, we construct a feature vector that encodes the node type (depot, pickup, delivery, or charging station), the spatial coordinates normalized to the unit square, the time window $[a_i, e_i]$ normalized by the planning horizon, the service time σ_i , and the load change q_i for pickups and deliveries. For each edge $(i, j) \in E$, we construct a feature vector containing the travel time δ_{ij} , the distance d_{ij} , and the energy consumption ε_{ij} expressed as a fraction of the battery capacity B . Since GREAT is only edge-based and does not operate on node features, we translate all node features into additional edge attributes as outlined by [36]. This is done by appending the node feature of a node $i \in V$ to all edge features \mathbf{h}_{ji} of edges $(j, i) \in E$ that lead to node i . Intuitively, this makes sense since, e.g., a load change q_i for visiting node i also corresponds to a load change q_i when traversing the graph from node j to i , i.e. taking edge (j, i) . Consequently, in total, each edge feature \mathbf{h}_{ij} captures information about edge $(i, j) \in E$ and node $j \in V$. As a result, we obtain a graph where all relevant information is encoded in the graph's edges. We note that all spatial features such as coordinates, distances, and times are normalized to the range $[0, 1]$ using instance-specific min-max scaling. This ensures that the attention weights remain consistent across problem instances of different scales and ensures stable learning.

The GREAT encoder consists of several stacked individual GREAT layers (in particular, we use the GREAT NB layer version of [36]). Each layer consists of an edge-based multi-head attention sublayer, a feed forward layer, residual layers and normalizations. We refer the reader to [36] for details. Here it suffices to say that at each layer ℓ , the representation of edge (i, j) is updated by attending to neighboring edges that share an endpoint with it. Specifically, we compute

$$\tilde{\mathbf{h}}_{ij}^{(\ell+1)} = \text{LN} \left(\mathcal{E}_A \left(\mathbf{h}_{ij}^{(\ell)}, \{\mathbf{h}_{km}^{(\ell)} : k = i \text{ or } m = j\} \right) + \mathbf{h}_{ij}^{(\ell)} \right),$$

where $\mathbf{h}_{ij}^{(\ell)}$ denotes the feature vector for edge (i, j) at layer ℓ , and the edge attention mechanism \mathcal{E}_A aggregates information from all edges that share either the source node i or the target node j . The $\mathcal{LN}(\cdot)$ denote the layer normalization operator. This edge-focused information passing allows the model to learn which routing decisions are promising by directly comparing adjacent edges in the graph structure. Afterwards, the final representation of layer ℓ is computed as

$$\mathbf{h}_{ij}^{(\ell+1)} = \mathcal{LN} \left((\mathbf{W}' \sigma (\mathbf{W}'' \tilde{\mathbf{h}}_{ij}^{(\ell+1)} + \mathbf{b}'') + \mathbf{b}') + \tilde{\mathbf{h}}_{ij}^{(\ell+1)} \right),$$

Table 1

Summary of notation and symbols used in the Electric Dial-a-Ride Problem (E-DARP) formulation.

Symbol	Description
<i>Problem Structure</i>	
n	Number of requests
0	Depot node
$P = \{1, \dots, n\}$	Pickup nodes
$D = \{n + 1, \dots, 2n\}$	Delivery nodes
F	Charging stations
$V = \{0\} \cup P \cup D \cup F$	All nodes
$E \subseteq V \times V$	All edges
K	Number of vehicles
<i>Vehicle State</i>	
l_t^k	Number of passengers on board at step t
$b_t \in [0, 1]$	State of Charge (SoC) at step t
τ_t	Current time at step t
v_t	Current node at step t
<i>Node Properties</i>	
q_i	Passenger load change at node i
\bar{L}_i	Maximum ride time for request i
$[a_i, \ell_i]$	Time window at node i
σ_i	Service time at node i
<i>Edge Properties</i>	
δ_{ij}	Travel time on edge (i, j)
d_{ij}	Distance on edge (i, j)
ε_{ij}	Energy consumption on edge (i, j)
<i>Vehicle Parameters</i>	
Q	Passenger capacity
B	Battery capacity
P^c	Charging power function

where $\mathbf{W}', \mathbf{W}'', \mathbf{b}', \mathbf{b}''$ are trainable weights and σ is the ReLU activation function. After processing through all layers, we derive node embeddings by aggregating the representations of all incoming edges:

$$\mathbf{z}_i = \sum_{j \in V} \omega_{ji} \mathbf{h}_{ji}^{(L)}$$

where L is the number of attention layers and ω_{ji} is a learned attention score that reflects the significance of each edge feature $\mathbf{h}_{ji}^{(L)}$ for node i . This produces a matrix $\mathbf{Z} \in \mathbb{R}^{N \times d_h}$ where N is the total number of nodes and d_h is the embedding dimension. These node embeddings are afterwards passed on to the route decoder. We note that the edge embeddings produced by the GREAT encoder are subsequently aggregated into node embeddings. This transformation is necessary to reduce both memory requirements and the size of the action space during the decoding procedure. In particular, it reduces the representation from $\mathcal{O}(n^2)$ edge embeddings to $\mathcal{O}(n)$ node embeddings, enabling efficient autoregressive decoding over candidate next nodes. We emphasize that this aggregation is performed only after edge-level reasoning has been completed. Directly operating on node features from the outset is ill-suited for energy-aware routing problems, as it cannot faithfully represent asymmetric, direction-dependent costs such as energy consumption that varies with travel direction due to terrain gradients or traffic patterns.

3.2. Route Decoder

The decoder constructs routes step by step using an attention-based pointer mechanism. At each decision step t , the decoder produces a probability distribution over the next node to visit, conditioned on the current partial route and the operational state of the vehicle.

We first build a context-aware query vector $\mathbf{c}_t \in \mathbb{R}^{d_h}$ that captures the current situation. The query combines information from multiple sources through learned linear projections. We add the embedding of the current node

weighted by \mathbf{W}_{curr} , the depot embedding weighted by $\mathbf{W}_{\text{depot}}$, the average of all node embeddings weighted by $\mathbf{W}_{\text{graph}}$, the average of visited node embeddings weighted by $\mathbf{W}_{\text{visited}}$, a summary of visited nodes based on the mask weighted by \mathbf{W}_{mask} , and projections of the operational state variables. The operational state includes the current passenger load l_t , battery level b_t , and time τ_t , each projected through learned weight matrices \mathbf{W}_l , \mathbf{W}_b , and \mathbf{W}_t respectively. Formally, we compute

$$\begin{aligned} \mathbf{c}_t = & \mathbf{W}_{\text{curr}} \mathbf{z}_{v_t} + \mathbf{W}_{\text{depot}} \mathbf{z}_0 + \mathbf{W}_{\text{graph}} \bar{\mathbf{z}} + \mathbf{W}_{\text{visited}} \bar{\mathbf{z}}_{\text{visited}} \\ & + \mathbf{W}_{\text{mask}} \phi(M_t, \mathbf{Z}) + \mathbf{W}_l l_t + \mathbf{W}_b b_t + \mathbf{W}_t \tau_t, \end{aligned} \quad (7)$$

where \mathbf{z}_{v_t} is the embedding of the current node, \mathbf{z}_0 is the depot embedding, $\bar{\mathbf{z}} = \frac{1}{N} \sum_i \mathbf{z}_i$ is the mean of all node embeddings, $\bar{\mathbf{z}}_{\text{visited}} = \frac{1}{|\mathcal{V}_t|} \sum_{i \in \mathcal{V}_t} \mathbf{z}_i$ is the mean of visited node embeddings, and $\phi(M_t, \mathbf{Z})$ summarizes which nodes have been masked based on the current feasibility constraints.

For each candidate next node j , we compute an attention score that balances semantic compatibility with energy efficiency. The score consists of two terms. The first term measures how well node j fits the current context through the inner product of the query and a key vector derived from the node embedding. The second term penalizes energy-intensive transitions by subtracting a weighted energy consumption term. We compute

$$u_{v_t j} = \frac{1}{\sqrt{d_h}} \mathbf{c}_t^\top \mathbf{W}_k \mathbf{z}_j - \lambda \varepsilon_{v_t j},$$

where \mathbf{W}_k is a learned key projection matrix, $\varepsilon_{v_t j}$ is the normalized energy consumption from the current node to node j , and $\lambda > 0$ is a hyperparameter that controls the strength of the energy penalty.

To stabilize training and prevent extreme logit values, we apply hyperbolic tangent clipping to the scores. Specifically, we compute

$$\tilde{u}_{v_t j} = \kappa \tanh(u_{v_t j} / \kappa),$$

where κ is a clipping parameter. This transformation bounds the range of the scores while preserving their relative ordering. We combine the clipped scores with the feasibility mask to obtain the final action probabilities. If node j violates any constraint, the mask sets $M_t(j) = -\infty$, which ensures that node j receives zero probability after the softmax. The probability of selecting node j as the next action is

$$\pi_\theta(j \mid s_t) = \frac{\exp(\tilde{u}_{v_t j} + M_t(j))}{\sum_{k \in V} \exp(\tilde{u}_{v_t k} + M_t(k))}.$$

During training, we sample an action from this distribution to enable exploration. During evaluation, we select the action with the highest probability to obtain the best predicted route.

3.3. Feasibility Mask

This section describes how the constraints from Eq. (4) are enforced during solution construction through action masking. The feasibility mask ensures that the decoder only considers valid actions at each decision step. At time step t , we construct a mask $M_t \in \{0, -\infty\}^N$ that indicates which nodes are allowed. For each candidate next node j , we set $M_t(j) = -\infty$ if visiting node j would violate any operational constraint, and $M_t(j) = 0$ otherwise.

We enforce six categories of constraints. First, we prevent revisiting nodes and ensure correct pickup-delivery ordering. We block any node j that has already been served. For delivery nodes, we additionally check that the corresponding pickup has been completed. If node j is a delivery and its paired pickup has not been served, we block node j .

Second, we enforce vehicle capacity constraints. Let l_t denote the current passenger load and q_j denote the load change at node j . The load change is positive for pickups, negative for deliveries, and zero for the depot and charging stations. We block node j if the resulting load $l_t + q_j$ would fall outside the valid range $[0, Q]$.

Third, we enforce time window constraints. We compute the arrival time at node j as $\tau_t^{\text{arr}} = \tau_t + \delta_{v_t j}$, where τ_t is the current time and $\delta_{v_t j}$ is the travel time. Service can start at $t_j^{\text{start}} = \max(\tau_t^{\text{arr}}, a_j)$ where a_j is the earliest allowed service time. If we arrive early, we wait until the time window opens. We block node j if $t_j^{\text{start}} > \ell_j$, where ℓ_j is the latest allowed service time.

Fourth, we enforce battery constraints. Let b_t denote the current battery level and $\epsilon_{v_t j}$ denote the energy required to travel to node j . We maintain a small safety reserve ρ to prevent complete battery depletion. We block node j if $b_t - \epsilon_{v_t j} < \rho$. Additionally, we check whether the vehicle can reach the depot or a charging station after visiting node j . Let $r_j = \min_{k \in F \cup \{0\}} \epsilon_{jk}$ denote the minimum energy needed to reach a safe location from node j . We block node j if $b_t - \epsilon_{v_t j} - r_j < \rho$.

Fifth, we enforce operational rules that prevent undesirable behavior and improve solution quality. We block the depot if the vehicle currently carries passengers, as returning with passengers on board would leave requests incomplete. We prevent direct transitions between charging stations to avoid ineffective charging station hopping. We block charging stations immediately after leaving the depot to prevent unnecessary early charging. We also block charging stations when the vehicle carries passengers to avoid inconveniencing customers with charging stops.

Sixth, we manage the vehicle fleet. When a vehicle returns to the depot and unserved requests remain, we check how many vehicles have been used. If fewer than K vehicles have been deployed, we reset the time and battery level to start a new vehicle. If all K vehicles have been used, we block all nodes except the depot to force episode termination.

The computational complexity of constructing the mask is $O(N)$ per decision step, where N is the number of nodes. The time window and battery checks require computing arrival times and energy consumption for each candidate node, which takes constant time per node given precomputed travel times and energy costs. The overall mask construction is dominated by vectorized operations over all candidate nodes.

3.4. Reward Function

The reward function implements the objective from Eq. (4) within the deep reinforcement learning framework. Let \mathcal{X} denote a complete solution consisting of all vehicle routes. We define three component costs: energy consumption $J_e(\mathcal{X}) = \sum_k \sum_t \epsilon_{v_t^k v_{t+1}^k}$, waiting time $J_w(\mathcal{X}) = \sum_k \sum_t \max(0, a_{v_{t+1}^k} - \text{arrive}_{t+1}^k)$, and lateness at deliveries $J_l(\mathcal{X}) = \sum_k \sum_t \max(0, t_{t+1}^k - b_{v_{t+1}^k}) \mathbb{1}[v_{t+1}^k \in D]$. The total cost combines these components as $J(\mathcal{X}) = w_e J_e(\mathcal{X}) + w_w J_w(\mathcal{X}) + w_l J_l(\mathcal{X}) - w_c n_{\text{served}}(\mathcal{X})$, where w_e, w_w, w_l , and w_c are scalar weights balancing energy, waiting, lateness, and service reward, respectively. The sparse reward $\mathcal{R}(\mathcal{X}) = -J(\mathcal{X})$ is provided only at episode termination, focusing credit assignment on final solution quality rather than intermediate decisions.

4. Experimental Setup

This section evaluates the proposed approach on two case studies based on real-world ride-sharing data from San Francisco. Both case studies use transportation requests derived from the Uber GPS dataset [39], which contains approximately 1.2 million GPS logs recorded every 4 seconds from active Uber vehicles during one week in San Francisco in 2011. After removing invalid records and extracting pickup and dropoff locations, the processed dataset contains about 25,000 trips with daily request volumes ranging from 2,000 to 6,000. The dataset is split into training, validation, and test sets.

4.1. Problem Instances and Training

The first case study uses benchmark instances introduced by [8] to enable direct comparison with published results. These instances have been widely adopted in the E-DARP literature, allowing assessment of how close learned policies come to optimal or best-known solutions.

The benchmark instances use transportation requests from the Uber GPS dataset [39] for San Francisco's Civic Center area. The transportation network is extracted from OpenStreetMap, and charging station locations are obtained from the Alternative Fuels Data Center of the U.S. Department of Energy. Instance sizes range from 16 to 50 requests served by 2 to 5 vehicles. The benchmark defines five depot locations that coincide with five charging station locations, allowing vehicles to start, end, and recharge at the same facilities. The original benchmark considers three minimum state-of-charge thresholds (0.1, 0.4, and 0.7) to study battery management under different safety margins. We evaluate only the 0.1 threshold, which represents the most realistic operational scenario with minimal safety buffer.

The benchmark objective differs from the formulation in Section 2.3. Rather than minimizing energy, waiting time, and tardiness, the benchmark minimizes travel time and tardiness with weights $w_1 = 0.75$ for travel time and $w_3 = 0.25$ for tardiness ($w_2 = 0$ for waiting time). Additionally, the benchmark formulation does not include the completion bonus term, implicitly assuming all requests must be served. We adopt these objective weights and constraint specifications to ensure direct comparability with published results.

Training instances for Case Study 1 are generated following these same specifications, sampling requests from the processed Uber GPS dataset. The neural network is trained using REINFORCE [40] with POMO augmentation [22] to increase variance and improve solution quality. To evaluate generalization across problem scales, we employ mixed-size training with instances containing $n \in \{16, 24, 32, 40, 50\}$ request pairs, sampled uniformly during training. The training dataset consist of 5000 graphs, the validation dataset of 1000 graphs, and the test dataset of the benchmark cases.

The second case study focuses on larger problem instances ranging from 100 to 250 request pairs, representing more realistic operational scenarios for urban ride-sharing services. While not yet approaching the thousands of daily trips characteristic of full-scale deployments, these instances incorporate realistic energy consumption modeling, expanded service areas, and modern electric vehicle specifications that better reflect practical fleet operations. This scale remains tractable for evaluation and analysis while demonstrating the approach's viability for problems where exact optimization methods become computationally prohibitive.

Transportation requests are drawn from the Uber GPS dataset [39] covering a broader region of San Francisco beyond the Civic Center area. The transportation network is extracted from OpenStreetMap [41], providing detailed road topology and connectivity. This network is augmented with elevation data from OpenTopography [42] to account for San Francisco's hilly terrain. Energy consumption is computed using a physics-based model that considers vehicle speed, acceleration, road grade, and powertrain efficiency, following the approach of [43]. The model accounts for both traction energy requirements and regenerative braking on downhill segments, providing substantially more realistic energy dynamics than the simplified linear models in Case Study 1.

Fleet configurations represent modern electric vehicle specifications with battery capacities of 20 and 40 kWh, fleet sizes of 4 and 8 vehicles, and ride-sharing capacities of 1, 2, and 3 passengers. Charging dynamics follow the nonlinear charging curve defined in Eq. (5), based on empirical data from [44]. Ten charging stations are placed at fixed locations in the Downtown and Civic Center districts for consistency across instances. Time windows are set to 15 minutes for both pickups and deliveries, providing moderate flexibility while maintaining realistic service quality requirements.

The objective function uses the full formulation from Section 2.3, incorporating energy consumption (w_e), waiting time (w_w), lateness (w_l), and completion bonus (w_c) with weights balanced to reflect operational priorities. Unlike the benchmark instances in Case Study 1 where all requests must be served, this formulation explicitly accounts for resource-constrained scenarios where battery capacity or fleet size may be insufficient to complete all demand.

For training on larger instances in Case Study 2, curriculum learning is employed to address computational challenges. Training directly on large instances is slow due to problem complexity and GPU memory constraints that force smaller batch sizes. Training begins with a model trained on $n = 100$ request pairs and progressively fine-tunes it on larger instances, increasing by 20% at each step: [100, 120, 144, 173, 207, 250]. For each instance size, a dataset of 2,000 instances is created and the model is fine-tuned for five epochs with POMO rollout of 100 trajectories. This few-shot approach leverages knowledge from the base model to adapt efficiently to larger problem scales without the computational expense of training from scratch.

For both case studies, the Adam optimizer [45] is used and POMO augmentation is applied by generating multiple parallel rollouts from different initial conditions for each training instance. All training and inference experiments were conducted on the Alvis cluster, a national computing resource provided by the Swedish National Academic Infrastructure for Supercomputing (NAIIS) and dedicated to artificial intelligence and machine learning research. Experiments were performed using NVIDIA A40 GPUs. This hardware configuration was used consistently across all reported experiments to ensure fair comparison of computational performance.

4.2. Baseline Methods

The proposed approach is compared against several baseline methods representing different algorithmic paradigms. Specifically, we compare against: (1) a greedy nearest-neighbor heuristic [46], which establishes a lower performance bound and quantifies gains from learned policies over myopic decision-making; (2) Adaptive Large Neighborhood Search (ALNS), the dominant metaheuristic paradigm for vehicle routing problems [47], providing a strong optimization baseline with practical computational requirements; and (3) exact methods including branch-and-price and branch-and-cut, which establish upper bounds on achievable solution quality. Together, these baselines span the spectrum from fast construction heuristics to computationally intensive exact solvers, enabling comprehensive evaluation of both solution quality and computational efficiency.

Greedy heuristic. We include a greedy heuristic to establish a lower performance bound and quantify the benefit of learned policies over myopic, rule-based decision-making. A nearest-neighbor greedy heuristic is implemented that constructs routes by iteratively selecting the closest feasible node from the current location. At each decision point, the heuristic evaluates all feasible nodes (those satisfying capacity, battery, time window, and precedence constraints) and selects the one with minimum energy consumption. When the current vehicle cannot feasibly serve any remaining requests, it returns to the depot and a new vehicle is initialized if the fleet limit allows.

ALNS. Adaptive Large Neighborhood Search represents the state-of-the-art metaheuristic paradigm for vehicle routing problems [47], providing a strong optimization baseline that balances solution quality with practical computational requirements. ALNS has been successfully applied to dial-a-ride variants, including static DARP with service quality objectives [48] and dynamic E-DARP with predictive routing [49]. We adapt the ALNS framework for our static E-DARP setting, incorporating destroy and repair operators suited to the pickup-delivery structure and battery constraints.

We benchmark our DRL policy against an ALNS heuristic with a maximum runtime of 2 hours per instance. ALNS starts from a feasible greedy rollout and iteratively improves the solution through destroy-repair cycles. In each iteration, a subset of pickup-delivery requests is removed from the current route and reinserted to reconstruct a complete solution. Feasibility and objective evaluation are performed by replaying candidate routes in the E-DARP environment, which enforces time windows, precedence, capacity, and battery constraints. The objective matches the E-DARP reward: a weighted sum of energy, waiting time, and late delivery penalties, plus completion reward.

We employ three destroy operators: random removal, which uniformly samples requests for deletion; Shaw removal [50], which removes clusters of related requests based on pickup and delivery travel times and time-window similarity; and worst removal, which targets requests whose removal yields the largest marginal improvement. For reconstruction, we use random insertion as well as regret- k insertion with $k \in \{2, 3\}$, where requests with the largest gap between their best and k -th best insertion position are prioritized [48].

Operators are selected via roulette-wheel sampling with adaptive weights updated every segment, following the weight adaptation scheme of [47]. We use rewards $\sigma_1 = 10$, $\sigma_2 = 5$, and $\sigma_3 = 1$ for discovering a new global best, improving the current solution, and accepting a non-improving solution, respectively. Weights are updated using exponential smoothing with decay rate $\rho = 0.2$, and we enforce a minimum weight to preserve exploration.

For solution acceptance, we use record-to-record travel (RTR) [51], which accepts any solution within a tolerance of the best found so far. The initial tolerance is set to 5% of the initial solution cost and decays by a factor of 0.99 per iteration.

Exact methods (Case Study 1 only). Exact methods establish an upper bound on achievable solution quality, enabling precise quantification of the optimality gap of learned policies on standardized benchmarks. For Case Study 1, additional comparison is made against the results reported in [16], which include exact solutions obtained through column generation (CG), branch-and-price (B&P), and branch-and-cut (B&C) for smaller instances, and best-known solutions from advanced optimization techniques for larger instances.

5. Results and Discussion

5.1. Case Study 1: Benchmark Performance

This case study evaluates solution quality and computational efficiency on standard benchmark instances, comparing GREAT against three exact optimization methods: column generation (CG), branch-and-price (B&P), and branch-and-cut (B&C) from [16]. Table 2 presents solution quality gaps relative to best-known solutions alongside computation times.

GREAT achieves optimal or near-optimal solutions across all instances while providing substantial computational advantages. For u2-16, GREAT matches the proven optimal solutions found by B&P and B&C, whereas CG exhibits a 0.92% gap. All methods find optimal solutions for u3-30, demonstrating that the learned policy captures essential problem structure at this scale.

For u5-50, GREAT achieves a 0.40% gap compared to 0.05% for CG and B&P. While these exact methods yield marginally better solutions, B&C struggles with a 7.09% gap. GREAT thus outperforms B&C by 6.69 percentage points, indicating effective learning of routing and charging strategies. Importantly, the exact methods reached the two-hour time limit without proving optimality, whereas GREAT produces its solution in sub-second time.

Table 2

Solution quality and computation time comparison on benchmark instances. Methods compared: Column Generation (CG), Branch & Price (B&P), Branch & Cut (B&C), and GREAT. Gap computed as percentage deviation from best-known solution: $\text{Gap\%} = 100 \times (z - z^*)/z^*$. Exact methods terminated at 7,200-second limit for u5-50.

Instance	CG		B&P		B&C		GREAT	
	Gap%	Time (s)	Gap%	Time (s)	Gap%	Time (s)	Gap%	Time (s)
u2-16 (16 requests)	0.92	43.6	0.00	22.2	0.00	21.0	0.00	<1.0
u3-30 (30 requests)	0.00	570.8	0.00	570.8	0.00	438.0	0.00	<1.0
u5-50 (50 requests)	0.05	7200.0 [†]	0.05	7200.0 [†]	7.09	7200.0 [†]	0.40	<1.0

[†]Time limit reached without proven optimality

Table 3

Performance comparison on E-DARP test instances (250 requests, 10 vehicles, averaged over 20 graphs). Best results are shown in bold.

Category	Metric	Greedy	ALNS	GREAT (Ours)
Solution Quality	Test Profit	209.45	847.07	927.25
	Completion Rate (%)	24.0	94.6	100.0
	Requests Served	60/250	236.5/250	250/250
Fleet Utilization	Vehicles Used	10.0	9.4	8.25
	Load Factor	1	1	1.94
	Charge Visits	11.8	1.25	0.45
	Energy per Vehicle (kWh)	3.2	11.6	9.6
Service Quality	Wait per Request (s)	168.6	8.3	33.2
	Lateness per Request (s)	35.4	0.0	30.3
Computational	Computation Time (s)	3.0	7200.0	0.01

The computational advantage of GREAT increases with problem size. For u2-16, GREAT achieves a 21 \times to 44 \times speedup over exact methods. For u3-30, this advantage grows to over 400 \times , with GREAT responding in under one second compared to approximately ten minutes for exact methods. For u5-50, all exact methods reach the 7,200-second limit while GREAT maintains sub-second inference, representing over 7,200 \times speedup at 0.40% optimality gap.

These results demonstrate that the neural approach scales more favorably than exact methods, which exhibit exponential growth in computation time. The consistent sub-second response time across all instance sizes confirms computational stability essential for real-time deployment. The trade-off of a small optimality gap for several orders of magnitude speedup represents a practical compromise suitable for dynamic operational environments.

5.2. Case Study 2: Scalability Analysis

5.2.1. Curriculum Learning

To assess the scalability of our approach to larger problem instances, we evaluate the curriculum-trained reinforcement learning policy on a challenging test scenario of 250 requests and 10 electric vehicles. The policy was progressively trained from 100 to 250 request pairs. We compare against two established baseline methods: a greedy nearest-neighbor heuristic that myopically assigns vehicles to the closest feasible requests, and an Adaptive Large Neighborhood Search (ALNS) metaheuristic with a computational budget of 2 hours per instance. ALNS is a state-of-the-art optimization method widely used for vehicle routing problems, combining multiple destroy and repair operators within a simulated annealing framework. Table 3 presents the comprehensive performance comparison across solution quality, fleet utilization, service quality, and computational efficiency metrics.

Our RL approach achieves the highest test profit of 927.25, outperforming ALNS by 9.5% (847.07) and greedy by 343% (209.45). Most notably, our method is the only one to achieve 100% completion rate, successfully serving all 250 requests, whereas ALNS achieves 94.6% completion (236.5 requests) and the greedy heuristic serves only 24% of requests (60 out of 250). This demonstrates that our learned policy effectively balances the complex trade-offs inherent in the E-DARP, including time window constraints, vehicle capacity, and battery management.

The RL approach demonstrates superior fleet utilization, requiring only 8.25 vehicles on average compared to 9.4 for ALNS and the full fleet of 10 for the greedy baseline. This 12% reduction in vehicles used compared to ALNS translates directly to operational cost savings. Furthermore, our method achieves a load factor of 1.94, indicating effective ridesharing with nearly two passengers transported simultaneously on average, whereas both ALNS and greedy achieve a load factor of 1, indicating single-passenger trips that underutilize vehicle capacity. The RL policy also learns efficient battery management, requiring only 0.45 charging station visits per route compared to 1.25 for ALNS and 11.8 for greedy. Despite serving all requests, RL consumes only 9.6 kWh per vehicle compared to 11.6 kWh for ALNS, demonstrating more energy-efficient routing. The greedy heuristic uses just 3.2 kWh per vehicle, but this low energy consumption reflects its poor completion rate rather than efficiency, as vehicles spend time traveling to charging stations rather than serving customers.

ALNS achieves the lowest wait and lateness times per request. However, this comes at the cost of serving fewer customers. ALNS effectively selects easier requests that can be served with minimal delay, leaving 13.5 requests (5.4%) unserved. Our RL approach prioritizes serving all customers and maximizing ride-sharing, accepting slightly higher average wait times (33.2s vs 8.3s) and lateness (30.3s vs 0.0s) as a trade-off for 100% completion and nearly 2× higher vehicle utilization.

Perhaps the most striking advantage of our approach is computational efficiency. The RL policy generates solutions in approximately 0.01 seconds per instance, representing a 720,000× speedup compared to ALNS which requires 7,200 seconds (2 hours) per instance. This dramatic difference stems from the fundamental nature of the approaches: ALNS performs iterative local search requiring thousands of solution evaluations, while our trained neural network performs a single forward pass to construct the solution. Even the simple greedy heuristic requires 3 seconds per instance due to repeated feasibility checking, making it 300× slower than our RL approach. This computational efficiency has significant practical implications for dynamic ride-sharing scenarios where customer requests arrive in real-time, as the ability to recompute solutions in milliseconds enables responsive fleet management and makes our approach suitable for deployment on edge devices with limited computational resources.

The strong scalability of the learned policy can be attributed to several architectural and methodological factors. First, the GREAT encoder’s edge-based attention mechanism directly models the routing decision space, learning which transitions are promising based on relational features rather than absolute positions. These learned patterns—such as prioritizing requests with tight time windows or balancing vehicle workloads—generalize across problem sizes because the underlying decision logic remains consistent regardless of instance scale. Second, curriculum learning enables the policy to progressively build competence on increasingly complex instances, transferring knowledge from smaller problems rather than learning large-scale coordination from scratch. Finally, inference requires only a single forward pass through the network, yielding polynomial-time complexity compared to the exponential growth in search space faced by exact methods and the iterative evaluation required by ALNS.

5.3. Hyperparameter Sensitivity Analysis

A comprehensive hyperparameter sensitivity analysis was conducted to identify the optimal neural architecture. In total, 10 configurations were evaluated by varying three key hyperparameters: hidden dimension $d \in \{64, 128, 192\}$, number of attention heads $h \in \{4, 8, 12\}$, and number of transformer layers $L \in \{4, 5, 6\}$. Experiments used a 4-vehicle fleet with 20 kWh batteries and 3-passenger capacity.

The best performing configuration achieved a maximum validation profit of 36048 at epoch 203 with $d = 192$, $h = 8$, $L = 6$, representing a **67.3%** improvement over the worst configuration, Table 4. However, $d = 128$ configurations offer an attractive middle ground: the $d = 128$, $h = 8$, $L = 5$ variant achieves competitive performance (35952 max profit, only 0.3% below the best) while converging quickly (95% of peak by epoch 36) and providing faster inference speed compared to $d = 192$ models. Fig. 3 shows the validation profit curves for all configurations, illustrating the convergence behavior across different hyperparameter settings. To quantify training stability, we report σ_{50} , the standard deviation of validation profit over the last 50 epochs, lower values indicate more consistent performance during the final training phase. Most configurations showed excellent stability with σ_{50} below 25. Notably, one configuration ($d = 192$, $h = 8$, $L = 5$) failed to converge, plateauing at a significantly lower profit level.

5.4. Sensitivity Analysis: Reward Function Weights

This subsection presents a sensitivity analysis examining how different reward function weight configurations affect system performance. The scenario is for 100 requests, 20 kWh battery and 8 vehicles. The reward function weights (w_e, w_w, w_l, w_c) control the relative importance of energy consumption, wait time, lateness, and completion

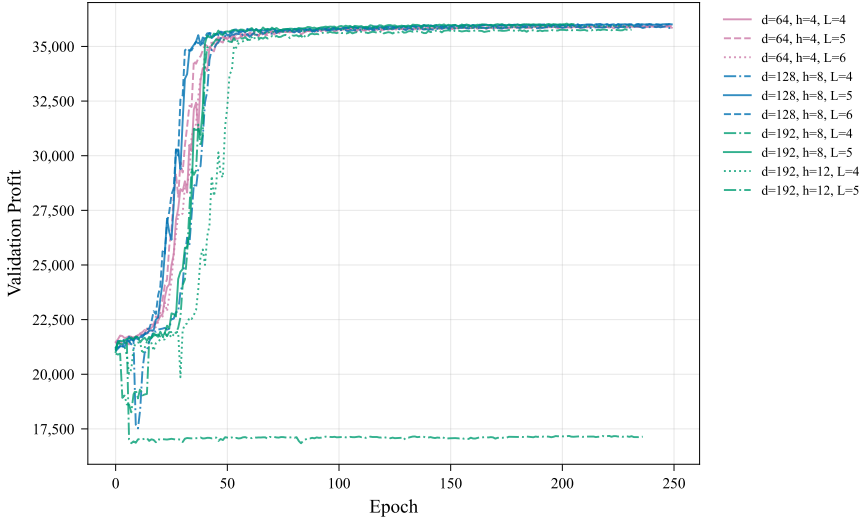


Figure 3: Validation profit over training epochs for all hyperparameter configurations. Most configurations converge to similar performance levels (~ 36000) by epoch 50, with $d = 128$ (blue) and $d = 64$ (purple) configurations showing comparable convergence rates. The $d = 192, h = 8, L = 5$ configuration (green dashed) diverged early and failed to recover.

Table 4

Hyperparameter sensitivity analysis results. Configurations are ordered by decreasing maximum validation profit. Best configuration shown in **bold**. d : hidden dimension, h : attention heads, L : transformer layers. $Ep_{95\%}$: epochs to reach 95% of max profit (convergence speed). σ_{50} : standard deviation over last 50 epochs (stability). Improv.: gain relative to worst configuration.

d	h	L	Max Profit	Epoch	Final Profit	$Ep_{95\%}$	σ_{50}	Improv. (%)
192	8	6	36048	203	36019	41	23.1	67.3
192	8	4	36031	218	36019	32	21.1	67.2
64	4	5	36026	221	36009	34	18.9	67.2
64	4	4	35969	234	35954	41	22.7	66.9
128	8	6	35956	219	35928	54	22.2	66.9
128	8	5	35952	249	35934	36	21.5	66.8
128	8	4	35921	244	35856	43	19.1	66.7
64	4	6	35920	235	35914	43	22.6	66.7
192	12	4	35793	229	35768	41	22.8	66.1
192	8	5	21548	6	17143	1	15.8	0.0

penalty terms respectively. Fig. 4 presents the training dynamics across all configurations, and Table 5 summarizes key operational and service quality metrics.

The sensitivity analysis reveals important trade-offs between completion incentives and operational cost penalties. As shown in Fig. 4(a), the baseline configuration (1, 1, 1, 1) with equal weights achieves 100% completion rate, utilizing 6.11 vehicles with an energy consumption of 7.10 kWh per vehicle and average wait time of 58 seconds per request.

Increasing the completion weight tenfold (1, 1, 1, 10) also achieves 100% completion. This configuration uses slightly more vehicles (6.15) with higher energy consumption (7.80 kWh) and comparable wait times (57 seconds). The stronger completion incentive encourages the policy to prioritize service fulfillment, resulting in slightly higher resource utilization as evident in Fig. 4(b).

However, scaling operational cost weights (10, 10, 10, 1) while maintaining unit completion weight produces suboptimal results. This configuration achieves only 74.0% completion rate despite utilizing all 8 vehicles. As illustrated in Fig. 4(c,e), the model exhibits significantly lower energy consumption (3.80 kWh per vehicle) and higher mean state-of-charge (86.9%), with longer wait times (64 seconds). The high operational penalties cause overly conservative

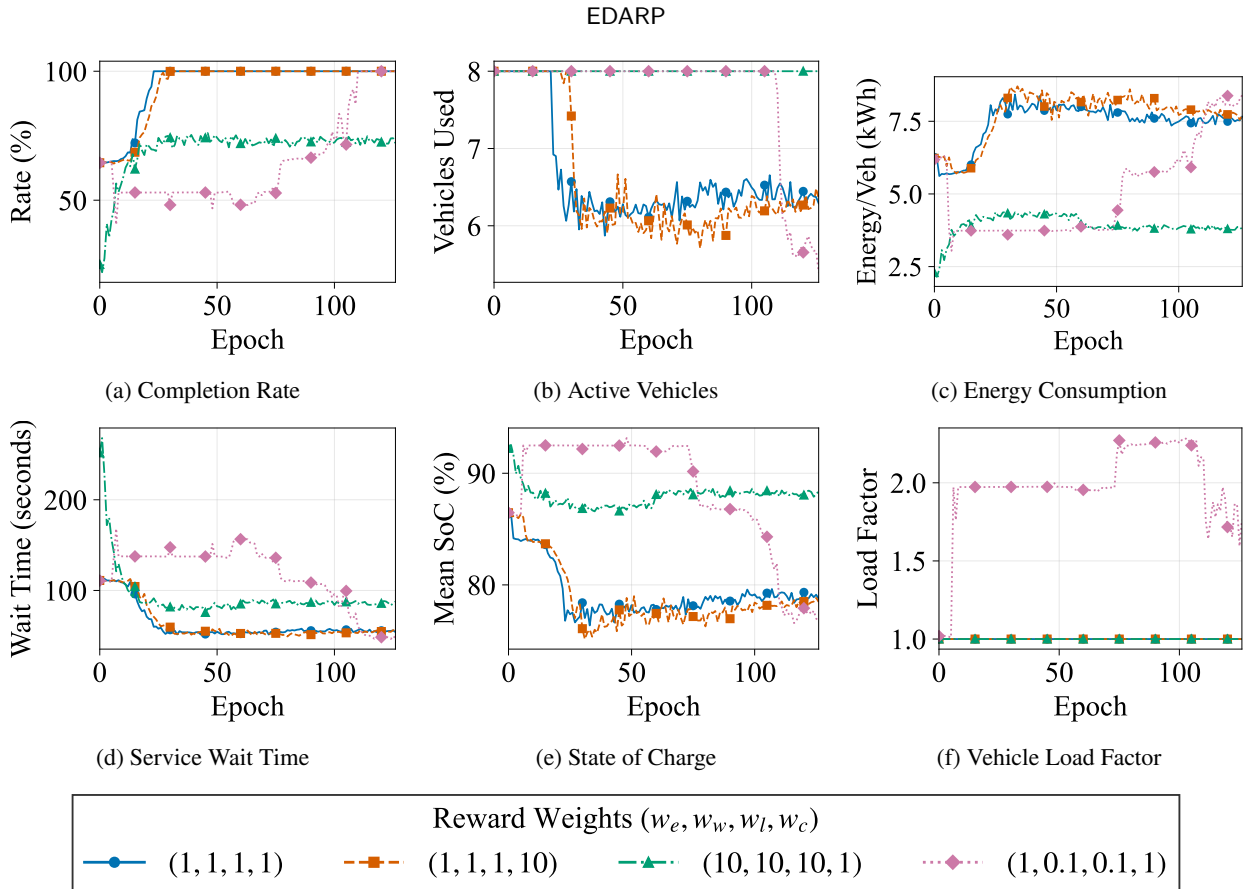


Figure 4: Reward weight sensitivity analysis.

Table 5

Reward weight sensitivity analysis: operational and service quality metrics. Weights are specified as (w_e, w_w, w_l, w_c) representing energy, wait time, lateness, and completion penalties respectively.

Reward Weights (w_e, w_w, w_l, w_c)	Completion Rate (%)	Vehicles Used	Load Factor	Energy/Veh (kWh)	Total Energy (kWh)	Mean SoC (%)	Wait Time (s)	Lateness (s)
(1, 1, 1, 1)	100.0	6.11	1.00	7.10	43.4	75.1	57.6	0.0
(1, 1, 1, 10)	100.0	6.15	1.00	7.80	48.0	76.8	57.0	0.0
(10, 10, 10, 1)	74.0	8.00	1.00	3.80	30.4	86.9	64.2	0.0
(1, 0.1, 0.1, 1)	100.0	5.61	1.82	8.30	46.6	76.8	48.9	39.7

behavior, with the policy prioritizing energy conservation and minimizing wait/lateness penalties over completing requests.

The configuration (1, 0.1, 0.1, 1) demonstrates an alternative trade-off by reducing the weights on wait time and lateness while maintaining equal emphasis on energy and completion. This configuration achieves 100% completion rate with the fewest vehicles (5.61) and a load factor of 1.82, compared to 1.0 for all other configurations. This difference is significant: a load factor of 1.0 indicates single-occupancy trips with no ride-sharing, while a load factor of 1.82 demonstrates that the policy has learned to pool multiple passengers per vehicle trip. The ride-sharing behavior results in lower average wait times (49 seconds vs. 57–64 seconds) due to more efficient vehicle utilization, but also leads to non-zero lateness (40 seconds mean) as vehicles make detours to serve multiple passengers. While the energy consumption per vehicle (8.30 kWh) is higher than the equal-weight configurations due to the increased workload from ride-sharing, the total fleet energy consumption (46.6 kWh) remains comparable to the baseline (43.4 kWh) and lower than the high-completion configuration (48.0 kWh).

Table 6

Sensitivity analysis results showing operational metrics at best-performing epochs. Bold values indicate best performance within each category.

Battery (kWh)	Fleet Size	Load Cap.	Val. Profit	Vehicles Used	Energy/Vehicle (kWh)	Total Energy (kWh)	Completion Rate (%)	Charge Visits	Load Factor
20	4	1	30,824	4.00	9.05	36.20	85.5	0.00	1.00
20	4	2	32,473	4.00	9.30	37.20	89.9	0.00	1.34
20	4	3	33,652	4.00	9.55	38.20	93.2	0.00	1.90
20	8	1	35,699	6.04	7.85	47.43	100.0	1.82	1.00
20	8	2	36,054	5.66	7.60	43.02	100.0	1.52	1.36
20	8	3	35,986	5.07	8.60	43.60	100.0	0.00	1.80
40	4	1	35,340	3.92	12.76	50.03	99.8	0.00	1.00
40	4	2	35,657	3.65	12.93	47.18	100.0	0.00	1.30
40	4	3	35,670	3.58	13.07	46.80	100.0	3.01	1.78
40	8	1	35,715	5.85	8.07	47.20	100.0	1.65	1.00
40	8	2	36,066	5.36	8.06	43.22	100.0	0.59	1.33
40	8	3	36,219	5.04	8.17	41.16	100.0	1.42	1.80

Table 7

Per-request service quality metrics (mean \pm standard deviation) at best-performing epochs. Bold values indicate lowest mean wait or lateness.

Battery (kWh)	Fleet Size	Load Cap.	Wait per Request Mean \pm Std (s)	Lateness per Request Mean \pm Std (s)
20	4	1	34.3 \pm 4.8	0.0 \pm 0.0
20	4	2	32.6 \pm 4.9	16.5 \pm 5.5
20	4	3	28.9 \pm 4.9	30.8 \pm 9.8
20	8	1	52.6 \pm 6.5	0.0 \pm 0.0
20	8	2	47.6 \pm 6.2	18.3 \pm 5.8
20	8	3	43.1 \pm 6.2	29.5 \pm 8.3
40	4	1	31.4 \pm 4.4	0.0 \pm 0.0
40	4	2	27.2 \pm 4.4	7.2 \pm 3.0
40	4	3	27.7 \pm 4.9	16.0 \pm 4.9
40	8	1	49.9 \pm 6.3	0.0 \pm 0.0
40	8	2	45.0 \pm 6.2	15.3 \pm 5.3
40	8	3	40.7 \pm 5.7	30.1 \pm 7.5

These results indicate that adequate completion weight is essential for achieving full service coverage. The baseline (1, 1, 1, 1) offers balanced operation with zero lateness but no ride-sharing, while the (1, 0.1, 0.1, 1) configuration enables ride-pooling behavior through reduced wait and lateness penalties. We adopt the (1, 0.1, 0.1, 1) configuration for subsequent experiments as it achieves full completion with efficient fleet utilization through ride-sharing, and the modest lateness trade-off is acceptable for the ride-pooling scenarios considered.

5.5. Sensitivity Analysis: Battery Size, Fleet Size and Ride-Sharing Capacity

This subsection examines how battery capacity, fleet size, and ride-sharing capacity affect system performance. We conduct the analysis on a 100-request scenario with 10 charging stations and 1 depot. The analysis considers battery capacities of 20 and 40 kWh, fleet sizes of 4 and 8 vehicles, and ride-sharing capacities of 1, 2, and 3 passengers per vehicle, yielding twelve configurations in total. Fig. 5 presents validation profit trajectories for all configurations, while Table 6 summarizes key operational metrics at best-performing epochs and Table 7 presents per-request service quality metrics.

All configurations demonstrate successful convergence, with best validation profits achieved between epochs 180 and 265 and final profits ranging from 30,824 to 36,219. Four-vehicle fleets with 20 kWh batteries require the longest training (189 to 219 epochs), reflecting challenging optimization under resource constraints. Eight-vehicle fleets converge more rapidly (180 to 190 epochs), benefiting from a more forgiving optimization landscape when sufficient resources exist. The configuration with 40 kWh batteries, 4 vehicles, and three-passenger capacity requires the longest training (265 epochs), suggesting that combining moderate fleet size with high ride-sharing capacity creates

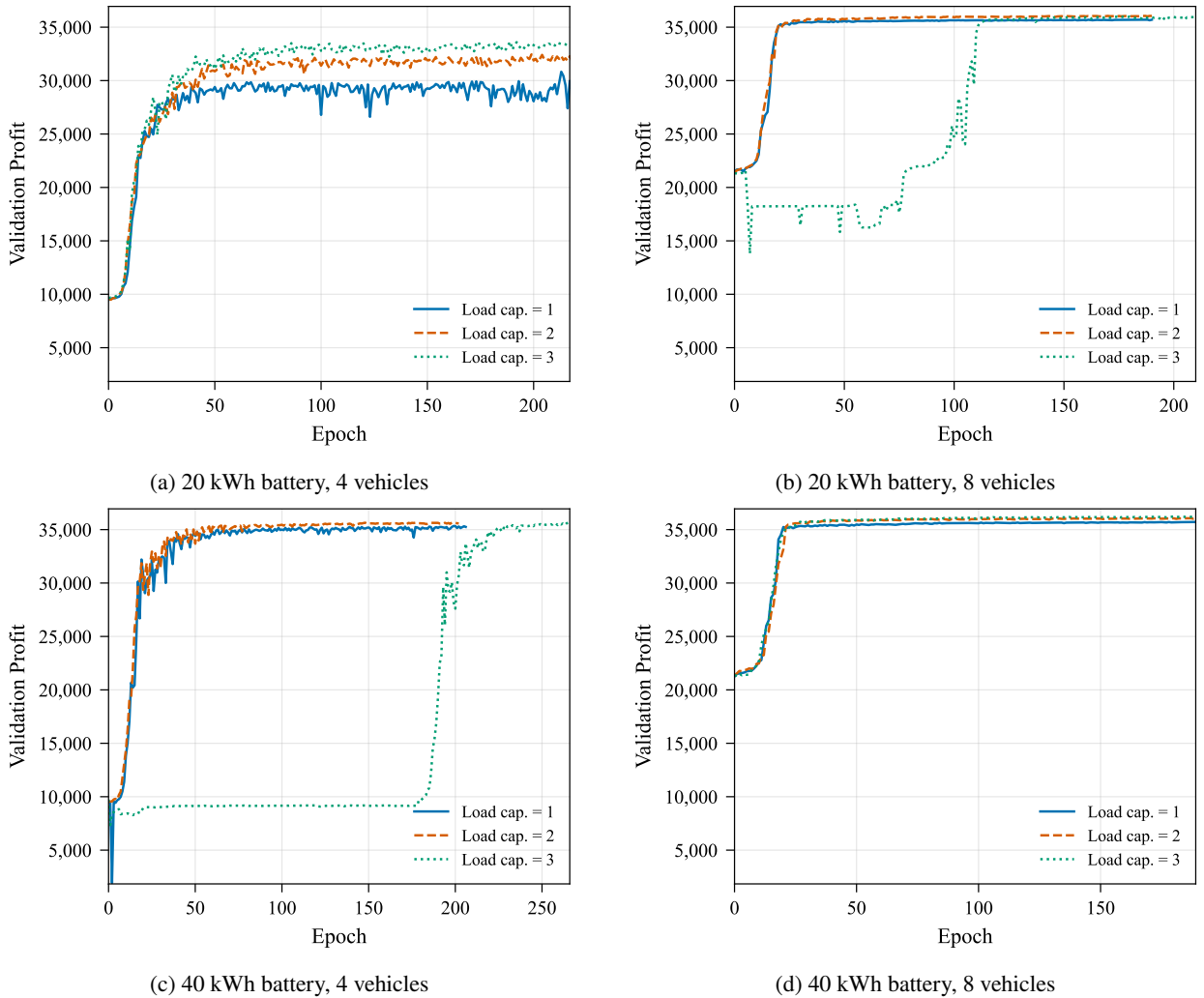


Figure 5: Validation profit convergence trajectories for all twelve configurations. Each subplot shows three ride-sharing capacity settings (1, 2, and 3 passengers per vehicle) for a given battery and fleet size combination.

a complex optimization landscape that warrants extended training budgets. Having established convergence across all configurations, we now examine how each parameter affects operational performance.

Fleet size emerges as the dominant factor for service coverage. All 8-vehicle configurations achieve 100% completion rates regardless of battery size or ride-sharing capacity, while 4-vehicle fleets with 20 kWh batteries reach only 85.5 to 93.2% completion. Larger fleets deploy 5.04 to 6.04 vehicles on average (63–76% utilization), preserving reserve capacity for demand fluctuations, whereas 4-vehicle fleets operate at 90–100% utilization. This reserve capacity also enables charging flexibility: 8-vehicle fleets with 20 kWh batteries utilize 1.52 to 1.82 charge visits since some vehicles can charge while others maintain service. Per-vehicle energy consumption is lower in larger fleets (7.60 to 8.60 kWh for 20 kWh batteries) compared to 4-vehicle fleets (9.05 to 9.55 kWh), indicating better load balancing with service demand spread more evenly. Total fleet energy consumption is higher for 8-vehicle configurations (41.16 to 47.43 kWh versus 36.20 to 50.03 kWh for 4 vehicles), reflecting the additional energy required to achieve complete service coverage. Load factors remain similar across fleet sizes for equivalent ride-sharing capacities.

Battery capacity has the greatest impact on resource-constrained fleets. For 4-vehicle configurations, increasing from 20 to 40 kWh improves completion rates from 85.5–93.2% to 99.8–100%, translating to profit improvements of 6–15%. Larger batteries enable better fleet utilization: 40 kWh configurations require fewer actively deployed

vehicles (3.58 to 3.92 versus 4.00 for all 20 kWh 4-vehicle cases), as individual vehicles can serve more requests per deployment cycle. Energy consumption per vehicle increases substantially with larger batteries (12.76 to 13.07 kWh versus 9.05 to 9.55 kWh), reflecting the ability to perform more work without charging interruptions. Notably, 4-vehicle configurations with 20 kWh batteries do not charge (0.00 visits) despite incomplete service coverage. This reflects a learned trade-off under severe capacity constraints: charging would temporarily remove scarce vehicles from service, and the resulting loss in service capacity outweighs the potential benefit of extended range. In contrast, 4-vehicle fleets with 40 kWh batteries only charge when ride-sharing is enabled (3.01 visits for 3-passenger capacity), as the combination of larger battery and ride-sharing creates scenarios where mid-operation charging becomes beneficial. For 8-vehicle fleets, battery capacity has minimal impact on completion rates since sufficient vehicles already ensure full coverage, though charging patterns differ: 40 kWh configurations require fewer charge visits (0.59 to 1.65) compared to 20 kWh configurations (0.00 to 1.82).

Ride-sharing capacity provides the most significant benefits in resource-constrained scenarios. For 4-vehicle fleets with 20 kWh batteries, completion rates improve from 85.5% (single occupancy) to 93.2% (three passengers), with corresponding profit gains of 9%. Load factors increase with capacity: 1.30–1.36 for two-passenger and 1.78–1.90 for three-passenger configurations, though these remain below theoretical maximums due to pickup and dropoff sequencing constraints. Ride-sharing also affects energy consumption patterns. Total fleet energy increases slightly with higher ride-sharing (36.20 to 38.20 kWh for 4-vehicle, 20 kWh configurations) as more requests are served, but for well-resourced configurations the opposite occurs: 8-vehicle fleets with 40 kWh batteries consume less total energy with ride-sharing enabled (41.16 kWh for 3 passengers versus 47.20 kWh for single occupancy) because fewer vehicle-kilometers are required when passengers share trips. For configurations that already achieve 100% completion, ride-sharing shows diminishing returns with profit improvements below 2%. The highest overall profit (36,219) is achieved with 40 kWh batteries, 8 vehicles, and three-passenger capacity, though this represents only 1.4% improvement over single occupancy (35,715). Wait times and lateness remain stable across all configurations regardless of ride-sharing capacity, with mean wait times ranging from 27 to 53 seconds and mean lateness below 31 seconds.

The interactions between these parameters reveal important trade-offs for E-DARP fleet design. Service coverage depends primarily on having sufficient vehicle capacity, achievable through either larger fleets or larger batteries, but the operational characteristics differ substantially. Larger fleets provide redundancy and charging flexibility at the cost of higher total energy consumption and capital investment, while larger batteries enable efficient operation with fewer vehicles but create longer charging windows when replenishment is eventually needed. Ride-sharing acts as a multiplier on existing capacity: it substantially improves performance when resources are constrained but offers marginal gains when the fleet is already sufficient. Energy efficiency is maximized through the combination of adequate fleet size and ride-sharing, which together enable lower per-vehicle utilization and shared passenger trips. Charging behavior emerges as a learned strategy that balances service availability against range extension, with the policy avoiding charging when vehicle scarcity makes the service interruption too costly. These results offer practical guidance for fleet operators: compact cities with moderate demand can use smaller fleets with larger batteries to reduce costs, while larger cities benefit from more vehicles that allow some to charge while others serve requests. Ride-sharing helps minimize total energy consumption and provides the greatest benefit when resources are limited. The learned policies' ability to adapt across these configurations shows their potential as planning tools for fleet sizing and vehicle selection.

5.6. Stochastic Energy Consumption and Travel Time

Real-world fleet operations face inherent uncertainty in travel times and energy consumption due to congestion, weather, and driver behaviour. To stress-test policy robustness under such uncertainty, we inject stochasticity directly into the environment during rollout: every time a vehicle commits to an arc (i, j) , the actual travel time and energy consumption are drawn from a half-normal distribution whose scale is 10% of the deterministic cost. Formally, letting δ_{ij} and ϵ_{ij} denote the deterministic estimates, we realize

$$\tilde{\delta}_{ij} = \delta_{ij} + |z| (0.1 \delta_{ij}), \quad (8)$$

$$\tilde{\epsilon}_{ij} = \epsilon_{ij} + |z| (0.1 \epsilon_{ij}), \quad (9)$$

with $z \sim \mathcal{N}(0, 1)$. The $|z|$ couples the two samples so that unusually long trips also consume more energy, while the half-normal form guarantees $\tilde{\delta}_{ij} \geq \delta_{ij}$ (vehicles cannot arrive earlier than the deterministic baseline without violating speed limits). Sampling happens online, after the route decision is made, which mirrors deployment: planners commit to deterministic estimates but discover the actual delay only after traversing the edge.

Table 8

Performance comparison under stochastic evaluation (10% half-normal noise). Both models are evaluated on 2000 instances with stochastic travel times and energy consumption.

Metric	Deterministic Training	Stochastic Training
<i>Primary Metrics</i>		
Average Reward	17.94	17.94
Completion Rate (%)	100.00	100.00
Total Waiting Time	0.063	0.065
Total lateness	0.022	0.023
<i>Fleet Utilization</i>		
Vehicles Used	6.45	6.63
Charging Visits	1.50	1.11
Low SoC Blocks	4.07	2.65
Fleet Exhausted (%)	4.8	11.0
<i>Energy Statistics</i>		
Mean SoC	0.766	0.773
Energy Used	2.62	2.61

We treat vehicles sequentially in a rolling re-plan scheme. After a vehicle completes its stochastic route, the dispatcher observes the realized energy consumption and travel times, quantities that were uncertain at the time of assignment, along with which pickups and deliveries were actually served. The next vehicle is then re-optimised using this revealed information. In effect, later vehicles benefit from a form of look-ahead: uncertainty that would still be unresolved in a fully simultaneous dispatch has already materialised by the time their routes are planned. This sequential revelation of stochastic outcomes provides an optimistic benchmark, yet it mirrors practical operations where new assignments are issued only after previous trips finish and is consistent with re-optimisation workflows when time windows are tight.

To study whether explicit exposure to uncertainty helps, we compare two training regimes: one where the model is trained purely on deterministic data, and one where the half-normal sampling is enabled throughout training so every trajectory experiences online noise. Both policies are evaluated on 2000 stochastic validation instances, with results reported in Table 8.

The results reveal that both training regimes achieve nearly identical performance under stochastic evaluation. The deterministic-trained policy attains an average reward of 17.94 with a completion rate of 100.00%, matching the stochastic-trained policy. This suggests that deterministic training already produces policies that are robust to moderate (10%) variability in travel times and energy consumption.

Interestingly, the two policies exhibit different operational strategies. The stochastic-trained model uses slightly more vehicles on average (6.63 vs 6.45) but makes fewer charging visits (1.11 vs 1.50). This indicates that exposure to uncertainty during training encourages more conservative battery management: the policy learns to maintain higher state of charge levels to buffer against unexpected energy consumption, reducing the need for en-route charging. This is further evidenced by the lower frequency of low SoC blocking events (2.65 vs 4.07) and slightly higher mean SoC (0.773 vs 0.766) for the stochastic-trained model.

However, the more conservative strategy comes with a trade-off: the stochastic-trained policy exhausts the vehicle fleet more frequently (11.0% vs 4.8% of instances). By deploying more vehicles with fewer charging stops, the policy occasionally runs out of fleet capacity before completing all requests, though this does not significantly impact the overall completion rate due to the sequential re-planning scheme.

These findings suggest that for moderate levels of uncertainty, deterministic training provides sufficient robustness. The learned policies generalize well to stochastic conditions without requiring explicit exposure to noise during training. This has practical implications: operators can train models on deterministic historical data and still expect reliable performance under real-world variability.

6. Conclusion

This paper presents a deep reinforcement learning framework for the Electric Dial-a-Ride Problem (E-DARP), addressing the operational challenges of autonomous electric vehicle fleets serving on-demand mobility requests. The

GREAT encoder architecture proves particularly well-suited for E-DARP by operating directly on edges rather than deriving edge information from node coordinates. This design naturally handles the non-Euclidean nature of energy-aware routing, where edge features such as travel times and energy consumption depend on factors like road gradient and traffic conditions that cannot be captured by coordinate-based distance calculations. The edge-centric formulation enables the policy to represent asymmetric costs, asymmetric real world energy consumption, and asymmetric graph structures.

Benchmark experiments against exact methods demonstrate that the learned policy achieves near-optimal solutions, with 0.00% optimality gaps on small instances (16 requests) and 0.40% gaps on larger instances (50 requests). The framework provides computational speedups of 21 to 44 times for small instances and over 7,200 times for instances where exact methods approach their time limits.

Curriculum learning enables scaling to 250-request instances, where the policy outperforms ALNS by 9.5% in solution quality while achieving 100% completion and 720,000 times faster computation. The learned policy exhibits emergent ridesharing behavior with 3.5 times higher vehicle utilization than ALNS, demonstrating effective multi-passenger coordination.

Hyperparameter sensitivity analysis reveals that smaller transformer architectures (hidden dimension 64–128) outperform larger models while exhibiting stable convergence, enabling efficient deployment without sacrificing solution quality. The reward function analysis confirms that adequate completion weight is essential for achieving full service coverage.

Sensitivity analysis across twelve configurations on 100-request scenarios reveals critical operational trade-offs and demonstrates the framework’s utility as a fleet planning tool. Battery capacity emerges as the dominant factor for resource-constrained fleets, with larger batteries enabling near-complete service coverage. Fleet size proves critical for service reliability, with larger fleets achieving full completion while maintaining reserve capacity for demand fluctuations. Ride-sharing provides the greatest benefit when resources are limited but shows diminishing returns when fleet capacity is sufficient. Service quality metrics remain stable across all configurations, with mean wait times below one minute and minimal lateness. These results illustrate how the framework can guide fleet sizing and vehicle selection decisions for different urban contexts.

Several limitations suggest directions for future research. The framework assumes deterministic demand arrival patterns, whereas real-world operations face uncertain request arrivals, customer no-shows, and cancellations. Extending the methodology to handle dynamic demand through online learning or anticipatory policies would enhance operational reliability. Additionally, the formulation assumes a homogeneous fleet where all vehicles share identical battery capacity, passenger capacity, and energy consumption characteristics. Real-world fleets often comprise mixed vehicle types with varying ranges and capacities, requiring extensions to handle heterogeneous vehicle assignment and routing decisions.

This research demonstrates that edge-based deep reinforcement learning can effectively address complex vehicle routing problems with integrated operational decisions, achieving near-optimal performance with computational efficiency suitable for real-time deployment. The sub-second inference time enables deployment in dynamic environments where traditional optimization methods become computationally intractable. Beyond empirical performance, the edge-centric formulation offers a more structured representation of routing decisions by operating directly on graph edges rather than latent node embeddings. This added structural alignment with the underlying combinatorial problem may facilitate future theoretical analysis of learning dynamics, stability, and convergence properties of routing policies. While formal convergence guarantees for deep reinforcement learning remain an open challenge, the proposed architecture provides a promising foundation for such analysis. As cities worldwide pursue electrification and autonomous mobility services, the framework presented here provides both algorithmic advances and practical guidance for fleet deployment decisions.

7. Acknowledgement

This work was co-funded by Vinnova, Sweden through the project: Simulation, analysis and modeling of future efficient traffic systems. This work was in part supported by the Transport Area of Advance within Chalmers University of Technology. The computations were enabled by resources provided by the National Academic Infrastructure for Supercomputing in Sweden (NAISSL) at Chalmers e-Commons partially funded by the Swedish Research Council through grant agreement no. 2022-06725.

References

- [1] United Nations. World urbanization prospects: The 2018 revision. Technical report, Department of Economic and Social Affairs, Population Division, New York, 2018.
- [2] Felix Creutzig, Patrick Jochem, Oreane Y. Edelenbosch, Linus Mattauch, Detlef P. van Vuuren, David McCollum, and Jan Minx. Transport: A roadblock to climate change mitigation? *Science*, 350(6263):911–912, 2015.
- [3] International Energy Agency. Transport sector co2 emissions by mode in the sustainable development scenario, 2000-2030. Technical report, International Energy Agency, Paris, 2020.
- [4] Daniel J. Fagnant and Kara Kockelman. Preparing a nation for autonomous vehicles: opportunities, barriers and policy recommendations. *Transportation Research Part A: Policy and Practice*, 77:167–181, 2015.
- [5] Rick Zhang and Marco Pavone. Control of robotic mobility-on-demand systems: A queueing-theoretical perspective. *The International Journal of Robotics Research*, 35(1-3):186–203, 2016.
- [6] Marco Pavone, Stephen L. Smith, Emilio Frazzoli, and Daniela Rus. Robotic load balancing for mobility-on-demand systems. *The International Journal of Robotics Research*, 31(7):839–854, 2012.
- [7] Javier Alonso-Mora, Samitha Samaranayake, Alex Wallar, Emilio Frazzoli, and Daniela Rus. On-demand high-capacity ride-sharing via dynamic trip-vehicle assignment. *Proceedings of the National Academy of Sciences*, 114(3):462–467, 2017.
- [8] Claudia Bongiovanni, Mor Kaspi, and Nikolas Geroliminis. The electric autonomous dial-a-ride problem. *Transportation Research Part B: Methodological*, 122:436–456, 2019.
- [9] Jean-François Cordeau and Gilbert Laporte. A tabu search heuristic for the static multi-vehicle dial-a-ride problem. *Transportation Research Part B: Methodological*, 37(6):579–594, 2003.
- [10] Jean-François Cordeau. A branch-and-cut algorithm for the dial-a-ride problem. *Operations Research*, 54(3):573–586, 2006.
- [11] Kris Braekers, An Caris, and Gerrit K Janssens. Exact and meta-heuristic approach for a general heterogeneous dial-a-ride problem with multiple depots. *Transportation Research Part B: Methodological*, 67:166–186, 2014.
- [12] Stefan Ropke, Jean-François Cordeau, and Gilbert Laporte. Branch and cut and price for the pickup and delivery problem with time windows. *Transportation Science*, 43(3):267–286, 2009.
- [13] Timo Gschwind and Stefan Irnich. Effective handling of dynamic time windows and its application to solving the dial-a-ride problem. *Transportation Science*, 49(2):335–354, 2015.
- [14] Dominik Goeke. Granular tabu search for the pickup and delivery problem with time windows and electric vehicles. *European Journal of Operational Research*, 278(3):821–836, 2019.
- [15] Xiaochang Liu, Dujuan Wang, Yunqiang Yin, and T. C. E. Cheng. Robust optimization for the electric vehicle pickup and delivery problem with time windows and uncertain demands. *Computers & Operations Research*, 151:106119, 2023.
- [16] Yue Su, Nicolas Dupin, Sophie N. Parragh, and Jakob Puchinger. A branch-and-price algorithm for the electric autonomous dial-a-ride problem. *Transportation Research Part B: Methodological*, 186:103011, 2024.
- [17] Yoshua Bengio, Andrea Lodi, and Antoine Prouvost. Machine learning for combinatorial optimization: a methodological tour d’horizon. *European Journal of Operational Research*, 290(2):405–421, 2021.
- [18] Oriol Vinyals, Meire Fortunato, and Navdeep Jaitly. Pointer networks. *Advances in neural information processing systems*, 28, 2015.
- [19] Irwan Bello, Hieu Pham, Quoc V Le, Mohammad Norouzi, and Samy Bengio. Neural combinatorial optimization with reinforcement learning. In *International Conference on Learning Representations*, 2017.
- [20] Mohammadreza Nazari, Afshin Oroojlooy, Lawrence V Snyder, and Martin Takáć. Reinforcement learning for solving the vehicle routing problem. In *Advances in Neural Information Processing Systems (NeurIPS)*, 2018.
- [21] Wouter Kool, Herke van Hoof, and Max Welling. Attention, learn to solve routing problems! In *International Conference on Learning Representations (ICLR)*, 2019.
- [22] Yeong-Dae Kwon and Jinkyoo Choo. Pomo: Policy optimization with multiple optima for reinforcement learning. In *Advances in Neural Information Processing Systems (NeurIPS)*, 2020.
- [23] Jingwen Li, Yining Ma, Ruize Gao, Zhiguang Cao, Andrew Lim, Wen Song, and Jie Zhang. Heterogeneous attentions for solving pickup and delivery problem via deep reinforcement learning. *IEEE Transactions on Intelligent Transportation Systems*, 23(3):2306–2315, 2021.
- [24] Shaoqing Luo et al. Solving pick-up and delivery problems via deep reinforcement learning based symmetric neural optimization. *Expert Systems with Applications*, 251:124514, 2024.
- [25] Michael Schneider, Andreas Stenger, and Dominik Goeke. The electric vehicle-routing problem with time windows and recharging stations. *Transportation Science*, 48(4):500–520, 2014.
- [26] Merve Keskin and Bülent Çatay. Partial recharge strategies for the electric vehicle routing problem with time windows. *Transportation Research Part C: Emerging Technologies*, 65:111–127, 2016.
- [27] Rafael Basso, Balázs Kulcsár, Ivan Sanchez-Diaz, and Xiaobo Qu. Dynamic stochastic electric vehicle routing with safe reinforcement learning. *Transportation Research Part E: Logistics and Transportation Review*, 157:102496, 2022.
- [28] Cynthia Rudin. Stop explaining black box machine learning models for high stakes decisions and use interpretable models instead. *Nature Machine Intelligence*, 1(5):206–215, 2019.
- [29] Christoph Molnar. *Interpretable Machine Learning: A Guide for Making Black Box Models Explainable*. Lulu.com, 2020.
- [30] Alejandro Barredo Arrieta, Natalia Díaz-Rodríguez, Javier Del Ser, Adrien Bennetot, Siham Tabik, Alberto Barbado, Salvador Garcia, Sergio Gil-Lopez, Daniel Molina, Richard Benjamins, Raja Chatila, and Francisco Herrera. Explainable artificial intelligence (XAI): Concepts, taxonomies, opportunities and challenges toward responsible AI. *Information Fusion*, 58:82–115, 2020.
- [31] Ashish Vaswani, Noam Shazeer, Niki Parmar, Jakob Uszkoreit, Llion Jones, Aidan N Gomez, Łukasz Kaiser, and Illia Polosukhin. Attention is all you need. In *Advances in Neural Information Processing Systems (NeurIPS)*, volume 30, pages 5998–6008, 2017.
- [32] Claire Glanois, Paul Weng, Matthieu Zimmer, Dong Li, Tianpei Yang, Jianye Hao, and Wulong Liu. A survey on interpretable reinforcement learning. *Machine Learning*, 113:4041–4085, 2024.

[33] Erika Puiutta and Eric M. S. P. Veith. Explainable reinforcement learning: A survey. In *Machine Learning and Knowledge Extraction (CD-MAKE)*, volume 12279 of *Lecture Notes in Computer Science*, pages 77–95. Springer, 2020.

[34] Reuben Narad, Léonard Boussoux, and Michael Wagner. Mechanistic interpretability for neural TSP solvers. In *NeurIPS 2025 Workshop on MLxOR: Mathematical Foundations and Operational Integration of Machine Learning for Uncertainty-Aware Decision-Making*, 2025.

[35] Andrew Silva, Matthew Gombolay, Taylor Killian, Ivan Jimenez, and Sung-Hyun Son. Optimization methods for interpretable differentiable decision trees applied to reinforcement learning. In *Proceedings of the Twenty Third International Conference on Artificial Intelligence and Statistics (AISTATS)*, volume 108 of *Proceedings of Machine Learning Research*, pages 1855–1865. PMLR, 2020.

[36] Attila Lischka, Filip Rydin, Jiaming Wu, Morteza Haghir Chehreghani, and Balázs Kulcsár. A great architecture for edge-based graph problems like tsp. *arXiv preprint arXiv:2408.16717*, 2025.

[37] Timothy M Sweda, Irina S Dolinskaya, and Diego Klabjan. Adaptive routing and recharging policies for electric vehicles. *Transportation Science*, 51(4):1326–1348, 2017.

[38] Victor Pillac, Michel Gendreau, Christelle Guéret, and Andrés L Medaglia. A review of dynamic vehicle routing problems. *European Journal of Operational Research*, 225(1):1–11, 2013.

[39] Uber Technologies Inc. Uber GPS dataset: Anonymized GPS logs from San Francisco. <https://github.com/dima42/uber-gps-analysis>, 2011. Accessed: 2024.

[40] Ronald J Williams. Simple statistical gradient-following algorithms for connectionist reinforcement learning. *Machine learning*, 8(3):229–256, 1992.

[41] OpenStreetMap contributors. Planet dump retrieved from <https://planet.osm.org>. <https://www.openstreetmap.org>, 2024.

[42] OpenTopography. OpenTopography: High-resolution topography data and tools. <https://opentopography.org>. Accessed: 2024.

[43] Rafael Basso, Balázs Kulcsár, Bo Egardt, Peter Lindroth, and Ivan Sanchez-Diaz. Energy consumption estimation integrated into the electric vehicle routing problem. *Transportation Research Part D: Transport and Environment*, 69:141–167, 2019.

[44] Nikolaos Wassiliadis, Jakob Schneider, Alexander Frank, Leo Wildfeuer, Xue Lin, Andreas Jossen, and Markus Lienkamp. Review of fast charging strategies for lithium-ion battery systems and their applicability for battery electric vehicles. *Journal of Energy Storage*, 44:103306, 2021.

[45] Diederik P. Kingma and Jimmy Ba. Adam: A method for stochastic optimization. In *3rd International Conference on Learning Representations, ICLR 2015*, San Diego, CA, USA, 2015.

[46] Daniel J. Rosenkrantz, Richard E. Stearns, and Philip M. Lewis. An analysis of several heuristics for the traveling salesman problem. *SIAM Journal on Computing*, 6(3):563–581, 1977.

[47] Stefan Ropke and David Pisinger. An adaptive large neighborhood search heuristic for the pickup and delivery problem with time windows. *Transportation Science*, 40(4):455–472, 2006.

[48] Christian Pfeiffer and Arne Schulz. An ALNS algorithm for the static dial-a-ride problem with ride and waiting time minimization. *OR Spectrum*, 44(1):87–119, 2022.

[49] Claudia Bongiovanni, Mor Kaspi, Jean-François Cordeau, and Nikolas Geroliminis. A predictive large neighborhood search for the dynamic electric autonomous dial-a-ride problem. In *9th Symposium of the European Association for Research in Transportation (hEART)*, 2020.

[50] Paul Shaw. Using constraint programming and local search methods to solve vehicle routing problems. In *International Conference on Principles and Practice of Constraint Programming*, pages 417–431. Springer, 1998.

[51] Gunter Dueck. New optimization heuristics: The great deluge algorithm and the record-to-record travel. *Journal of Computational Physics*, 104(1):86–92, 1993.